

Fine-scale prediction of biomass and leaf nitrogen content in sugarcane using UAV LiDAR and multispectral imaging



Yuri Shendryk^{a,*}, Jeremy Sofonia^b, Robert Garrard^{c,1}, Yannik Rist^a, Danielle Skocaj^d, Peter Thorburn^a

^a CSIRO, Agriculture and Food, Brisbane Australia

^b Emegent, Brisbane, Australia

^c CSIRO, Land and Water, Brisbane, Australia

^d Sugar Research Australia, Tully, Australia

ARTICLE INFO

Keywords:
Sugarcane
Nitrogen
Fertilizer
UAV
Drone
LiDAR
Multispectral
Biomass
Yield
NDVI
Fusion
PCA

ABSTRACT

Unmanned Aerial Vehicle (UAV) platforms and associated sensing technologies are extensively utilized in precision agriculture. Using LiDAR and imaging sensors mounted on multirotor UAVs, we can observe fine-scale crop variations that can help improve fertilizer management and maximize yields. In this study we used UAV mounted LiDAR and multispectral imaging sensors to monitor two sugarcane field trials with variable nitrogen (N) fertilization inputs in the Wet Tropics region of Australia. From six surveys performed at 42-day intervals, we monitored crop growth in terms of height, density and vegetation indices. In each survey period, we estimated a set of models to predict at-harvest biomass at fine scale (2 m × 2 m plots). We compared the predictive performance of models based on multispectral predictors only, LiDAR predictors only, a fusion of multispectral and LiDAR predictors, and a normalized difference vegetation index (NDVI) benchmark. We found that predictive performance peaked early in the season, at 100–142 days after the previous harvest (DAH), and declined closer to the harvest date. At peak performance (i.e. 142 DAH), the multispectral model performed slightly better ($\bar{R}^2 = 0.57$) than the LiDAR model ($\bar{R}^2 = 0.52$), with both outperforming NDVI benchmark ($\bar{R}^2 = 0.34$). This, however, flipped later in the season, with LiDAR performing slightly better than the multispectral imaging and NDVI benchmark. Interestingly, the fusion model did not perform significantly better than the multispectral model at 100–142 DAH, nor better than LiDAR in subsequent periods. We also estimated a model to predict contemporaneous leaf N content (%) using multispectral imagery, which demonstrated an \bar{R}^2 of 0.57. Our results are of particular interest to nutrient management programs aiming to deliver N fertilizer guidelines for sustainable sugarcane production, as both fine-scale biomass and leaf N content predictions are feasible when management interventions are still possible (i.e. as early as at 100 DAH).

1. Introduction

The primary goal of precision agriculture is to improve crop biomass production and fertilizer management, while reducing operating costs and environmental pollution (Chlingaryan et al., 2018). The potential growth and biomass of the crop depends on many different attributes such as soil properties, climate, topography, irrigation and fertilizer management. The need for timely and accurate sensing of these attributes over agricultural fields has led to increased adoption of both remote sensing technologies (Mulla, 2013) and simulation models (Jones et al., 2017; Keating and Thorburn, 2018) in precision agriculture.

Although there are several simulation models for crop biomass and nitrogen status estimation (Holzworth et al., 2014; Kroes et al., 2008), they are not widely and efficiently used due to a large number of data requirements (e.g. types of soils, climates and management practices, etc.). Instead, remote sensing technologies are becoming more widely used in building decision support tools to improve biomass production and fertilizer management. While satellite remote sensing applications in agriculture have focused on a wide range of applications across different crop systems, including biomass (Rembold et al., 2013) and nutrient content prediction (Abdel-Rahman et al., 2013), Unmanned Aerial Vehicle (UAV) based remote sensing has gained substantial

* Corresponding author.

E-mail address: yuri.shendryk@csiro.au (Y. Shendryk).

¹ Codes and data for reproducing results in this article can be found at github.com/RobGarrard/Fine-scale-prediction-of-leaf-nitrogen-content-and-yield-in-sugarcane.

traction in recent years due to lower operational costs, operational flexibility and higher spatial resolution of imagery (Matese et al., 2015). Moreover, UAV-based sensors are less prone to the challenges of satellite-based sensors, such as atmospheric absorption and angles of image capture.

UAV platforms and associated sensing technologies are a rapidly developing field being extensively used in precision agriculture and farming. Using remote sensing sensors mounted on multirotor or fixed wing UAVs, fine-scale variations in crops growth may be observed (Sofonia et al., 2019b; Christiansen et al., 2017; Bendig et al., 2015) that can improve the efficiency of fertilizer inputs and maximize yields. Nitrogen (*N*) is a major nutrient for plant growth due to its role in the process of photosynthesis (Andrews et al., 2013), and an estimate of its content (%) in leaves can be used as an indicator of *N* deficiency in plants (Romheld, 2012; Calcino et al., 2018). Similarly, crop biomass is one of the main metrics used to determine the efficiency of food production and its accurate prediction is needed for efficient management of the fertilization and to inform milling and harvest programs. Hence, the prediction of both leaf *N* content and biomass for different crops has become a subject of many UAV-based precision agriculture studies.

The application of UAV-derived multispectral, hyperspectral and thermal imagery as well as their derivative structure from motion (SfM; a.k.a. photogrammetry) point clouds have been widely used in precision agriculture (Zhang and Kovacs, 2012; Nex and Remondino, 2014; Gago et al., 2015; Adão et al., 2017; Duan et al., 2017). For example, multispectral imaging has been previously applied to estimate leaf *N* content in wheat (Zheng et al., 2018b) and rice (Zheng et al., 2018a). It was also demonstrated that biomass could be reliably predicted (coefficient of determination (R^2) > 0.65) using UAV-derived multispectral and/or Red, Green and Blue (RGB) imagery in rice (Zhou et al., 2017), maize (Maresma et al., 2016), barley (Kefauver et al., 2017) and wheat (Schirrmann et al., 2016). Similarly, the application of photogrammetric methods for biomass prediction in crops is relatively well researched, for example, in barley (Bendig et al., 2014) and wheat (Holman et al., 2016).

In contrast, the application of UAV-based Light Detection and Ranging (LiDAR) sensors has been relatively limited in agricultural studies, mainly due to the higher financial costs associated with these systems. However, recent work by Christiansen et al. (2017) and Sofonia et al. (2019b) demonstrated its applicability in monitoring wheat and sugarcane crops, respectively, showing significant correlations between LiDAR-derived crop attributes and biomass. Furthermore, Sofonia et al. (2019b) highlighted the advantage of using LiDAR over photogrammetric systems in dense crops like sugarcane, where SfM-derived height estimates yielded generally poor coefficient of determination ($R^2 \leq 0.32$) in predicting biomass. This was mainly due to limited capacity of SfM-derived point clouds to derive reliable height estimates in sugarcane as early as at 142 days after the previous harvest (DAH). Finally, while the fusion of multispectral imagery and photogrammetry (Bendig et al., 2015) as well as hyperspectral imagery and LiDAR scans (Wang et al., 2017) has been previously reported to improve crop biomass predictions, the combined use of LiDAR with multispectral systems has not been reported in precision agriculture. The combined use of airborne LiDAR scans with either multispectral or hyperspectral imagery previously also confirmed to substantially improve the estimates of important forest attributes (e.g. biomass, cover types and health) (Luo et al., 2017; Shendryk et al., 2016; Meng et al., 2018), and we expect these results to be transferable to crop systems.

As previously noted, much of the previous work in UAV-based precision agriculture has been focused on estimating important agricultural attributes in staple or other widely grown crops (i.e. rice, wheat, maize, etc.). However, other crops, such as sugarcane, represent large and important rural industries in tropical countries including Brazil and India (FAO, 2019), where it is both a significant source of energy in human diets as well as biofuels. There are multiple stakeholders across the agricultural value chain interested in understanding

and forecasting supply in the sugarcane market (Everingham et al., 2007), including sugarcane growers, sugar mills, commodities traders, banks and insurance companies as well as biofuel producers. The efficient management of the fertilization and harvesting processes helps to increase profitability in the sugarcane sector. Therefore, an accurate model for sugarcane biomass and leaf *N* content is needed to manage sugar mills and allocate other stakeholders' resources.

Sugarcane is a semi-perennial crop, which in Australia typically grows for 12–18 months and reaches height of up to four meters before being mechanically harvested. After harvesting new ratoon crop emerges from the same root system. Since the yield decreases over time, the plants and the root system are generally removed after five years, and new crop is planted (Bull, 2000; Molijn et al., 2018). Indicatively, the growth of sugarcane follows five phenological phases: (1) germination – where the plant is established and tillers are initiated; (2) early growth – where the leaf canopy is established and maximum growth (i.e. 20–30 mm/day) or elongation of the sugarcane stem occurs; (3) maturation – where stem elongation slows down (i.e. 5–10 mm/day) and sugar storage or ripening dominates; (4) flowering – where vegetative growth ceases and a flower is produced; (5) ratooning – where stems are harvested and crop re-growth occurs from underground buds on the severed stems (Bull, 2000). Typically timing of *N* fertilization coincides with the germination phase of sugarcane development, while most *N* uptake occurs during early growth phase (Calcino et al., 2018).

Sugarcane supply can vary according to the cultivation area, climatic conditions and disease. Unfortunately, in most countries, sugarcane biomass predictions are often still performed through traditional methods that are site-specific and time-consuming (Promburom et al., 2001; Molijn et al., 2018). In the traditional system, sugarcane biomass is estimated based on the planting records or allometric models. These approaches often require visual interpretation by an experienced eye, and farmers' knowledge on historical production and environmental conditions (Bocca et al., 2015). Similarly, the common technique for estimation of sugarcane *N* status is often based on a destructive chemical analysis of leaf measurements, which is laborious, lengthy, and costly (Vigneau et al., 2011). Therefore, remote sensing has recently been proposed as an alternative approach to predict sugarcane biomass and leaf *N* content.

The majority of remote sensing studies to date have used satellite imagery to predict sugarcane biomass, but have had mixed success (Morel et al., 2014; Rahman and Robson, 2016). In contrast, the applications of UAV-based systems for this purpose are quite limited. For example, both Som-ard et al. (2018) and Sanches et al. (2018) used UAV-derived RGB imagery coupled with ground information to predict sugarcane biomass in Thailand and Brazil, respectively. To date, such studies have been relatively limited in their scope; often only examining the capabilities of UAV techniques during a single event (Som-ard et al., 2018; Sofonia et al., 2019b) or focusing on metrics other than biomass and leaf *N* content (e.g. quality, ground cover, height, etc.) (Luna and Lobo, 2016; Duan et al., 2017; De Souza et al., 2017). To our knowledge there are no studies attempting to estimate leaf *N* content in sugarcane using a UAV-based system, and most research in this space has been conducted using either in situ or satellite based hyperspectral imagery (Abdel-Rahman et al., 2013; Miphokasap et al., 2012; Miphokasap and Wannasiri, 2018).

Given the need for the development of accurate models able to predict sugarcane biomass and leaf *N* content using UAV-derived data at fine scale, the aims of this study were to: (1) test the ability of multispectral imagery in predicting leaf *N* concentrations, (2) create a predictive model allowing us to infer the stage at which it is possible to derive reliable at-harvest biomass predictions and (3) investigate benefits of fusing LiDAR and multispectral data for predicting sugarcane biomass. While for predicting leaf *N* concentrations we used multi-temporal, multispectral imagery only, the biomass prediction task was based on mono-temporal, multispectral and/or LiDAR data, as we aimed to determine the earliest pre-harvest point in time that can

reliably predict at-harvest biomass. In Sofonia et al. (2019b) we demonstrated that biomass in sugarcane could be estimated (R^2 of 0.71 ($n = 20$)) at the time of harvest using UAV-derived LiDAR scans at the scale of individual field blocks (i.e. 10 m × 30 m). However, biomass predictions generated at the time of harvest are not relevant to crop management. Therefore, fine-scale information (as early in the season as possible) on at-harvest biomass and leaf N status is needed, thus helping to arrange the logistics of harvesting, inform within field management and rectify N crop deficiency. Furthermore, if a sugarcane grower wanted to use a model for biomass prediction, inputs to such a model must be relatively cheap to obtain. A model that predicts at-harvest biomass based on the entire set of predictors across all time periods would require a grower to conduct multispectral and LiDAR surveys at several time periods throughout the growth cycle. Given this would be very costly, we instead aim to determine the accuracy with which we can predict at-harvest biomass based on a single UAV mission.

2. Methodology

2.1. Study area

The study area was located in the Tully river catchment in northeast Queensland, which has a tropical climate and is one of the wettest regions of Australia. An average annual rainfall here exceeds 4000 mm (Yu, 1998), 60% of which falls in the wet season from December to March. The region is highly agriculturally productive and has experienced substantial expansion over past decades in the production of bananas, pawpaw and other tropical fruits (Mitchell et al., 2007), and includes approximately 6.5% (381 km²) of the total sugarcane cultivation in Australia (5866 km²) (ABARES, 2018). Two sites with sugarcane (*Saccharum officinarum L.*) variety Q208_A planted in 2015 (i.e. 3rd ratoon in 2017) were selected for monitoring throughout the 2017–2018 growing season (Fig. 1). The sugarcane in Site #1 was planted on a well-drained alluvial soil with dark greyish brown silty light clay A horizon and brownish yellow medium clay with moderate fine blocky structure B horizon. In contrast, sugarcane in Site #2 was planted in a poorly-drained alluvial soil with brown silty clay loam A horizon and brownish grey medium clay coarse blocky structured B horizon mottled at depth.

2.2. Experimental design and field measurements

The design of the field experiments is presented in Fig. 2.² Five N treatments (0, 70, 110, 150, 190 kg N/ha) were replicated four times using a randomized complete block design. To train a good predictive model, data with variation in both leaf N content and biomass were necessary. Therefore, the experimental application of N exploited in this study was not used to estimate the treatment effect of N on biomass and leaf N content, as in previous works (Thorburn et al., 2011); but instead, as a source of variation in crop biomass and leaf N. Each block was 10 m wide, 30 m long and consisted of six sugarcane rows. The N treatments were applied 52 and 55 days after harvesting (DAH) the previous crop at Site #1 and Site #2, respectively (i.e. Site #1 and #2 were harvested on 11 and 8 of September 2017, respectively). The N fertilizer was applied as urea using a single row variable rate side dress fertilizer applicator.

To observe temporal variation in the growth of sugarcane from ratooning to harvest, six UAV Surveys were conducted every six weeks (42 days) from November 2017 until June 2018 (Table 1). The timing of this study was designed to commence following the harvest of the previous season's crop and emergence of shoots, with the final survey

undertaken prior to the mill harvest. All UAV flights were executed on the same day around the same time (i.e. midday) with the minimal presence of clouds in an effort to minimize variability in lighting exposure of the multispectral imagery between surveys and with Site #1 being always surveyed prior to Site #2.

To evaluate the potential utility of UAV LiDAR and multispectral imagery for predicting sugarcane biomass and leaf N content, physical samples were collected at different stages of crop development. Leaf N was measured during Surveys #2–5, while biomass sampling was performed during Survey #6 only (Table 1). Leaf sampling involved selecting leaves from stems of average height, sampling the third leaf from the top of the stem and collecting 40 leaves at random (Calcino et al., 2018) from across rows 2 and 5 of each N application block (Fig. 2). The third leaf from the top of the stem was selected for further analysis as it is close to the peak of foliar metabolic activity and is used by most countries for foliar diagnosis (Bakker, 2012). All samples were dried in an oven set at 60 °C, mulched and sent to Incitec Pivot Limited laboratory for analysis of nutrient concentrations. In total 40 samples (20 at each site) during four Surveys (#2–5) were collected. In contrast, biomass sampling was performed in 56 randomly distributed 2 m × 2 m plots along rows 1 and 6 (Fig. 2) immediately following Survey #6 (i.e. 7 weeks before the sugarcane was due to be harvested). Total, leaf, and stem (i.e. yield in sugarcane (Muchow et al., 1996)) fresh biomass (kg) as well as number of stems were measured in each 2 m × 2 m plot (Fig. 3). A Leica GS16 GNSS ‘Smart Antenna’ with CS20 Controller (Leica Geosystems, 2019) was used in combination with a connection to the Smartnet AUS RTK network to delineate each biomass sampling plot with a <20 mm 3D resolution.

In addition, another set of biomass measurements using the currently adopted standard (Muchow et al., 1993) for assessing sugarcane biomass in field experiments trials in Australia was performed by Sugar Research Australia (SRA) for Sites #1 and #2 on 30 and 26 July 2018, respectively. Stems were counted within 10 m of the center of rows 3 and 4 with 45 stems randomly collected and weighed as total fresh biomass (t/ha). Of these, 20 stems were again randomly selected and partitioned into stems and leaves. Leaves and stem biomass (i.e. yield in t/ha) were delineated between the 5th and 6th dewlaps for stems that had not flowered, and the 7th and 8th dewlaps for stems that presented flowering. Each component was then weighed separately and recorded. This data set was also used in Sofonia et al. (2019b) to regress UAV-derived LiDAR and SfM data with sugarcane stem biomass, while here we used it to validate our UAV-derived total biomass predictions.

2.3. UAV system and flight parameters

In this study we used a combination of LiDAR and multispectral imaging sensors mounted on a DJI M600 Pro multirotor UAV (Fig. 4) to monitor sugarcane N fertilizer rates field trials. The LiDAR scans were collected using an Emesent Hovermap payload (Emesent, 2019), which was integrated with the Velodyne VLP-16 sensor and processed using Simultaneous Localization and Mapping (SLAM) algorithm (Sofonia et al., 2019a,b). The Velodyne VLP-16 is a 16-channel dual-return sensor with a scan rate of up to 600 kHz, angular resolution (vertical) of 2°, field-of-view (FOV) along the z-axis of 360° × 30°, reported accuracy of 0.03 m and range of up to 100 m (Velodyne, 2018). In this study, VLP-16 sensor with the Emesent Hovermap configuration was able to generate point clouds with nominal point spacing (i.e. the “representative” distance between points) of 0.02 m and average point density of 2000 points/m². In contrast, multispectral imagery was obtained using a MicaSense RedEdge sensor (MicaSense, 2019). With five narrow spectral bands: Blue (475 nm center, 20 nm bandwidth), Green (560 nm center, 20 nm bandwidth), Red (668 nm center, 10 nm bandwidth), Red edge (717 nm center, 10 nm bandwidth), Near-infrared (840 nm center, 40 nm bandwidth). The small (9.4 × 6.3 × 4.6 cm) lightweight (0.18 kg) camera provided a 47.2° field of view, resolution of approximately 2 cm/pixel at 30 m altitude and frame rate of 0.5 Hz

² The experimental sites were established as part of Sugar Research Australia and the Department of Environment and Science funded project #2015065.

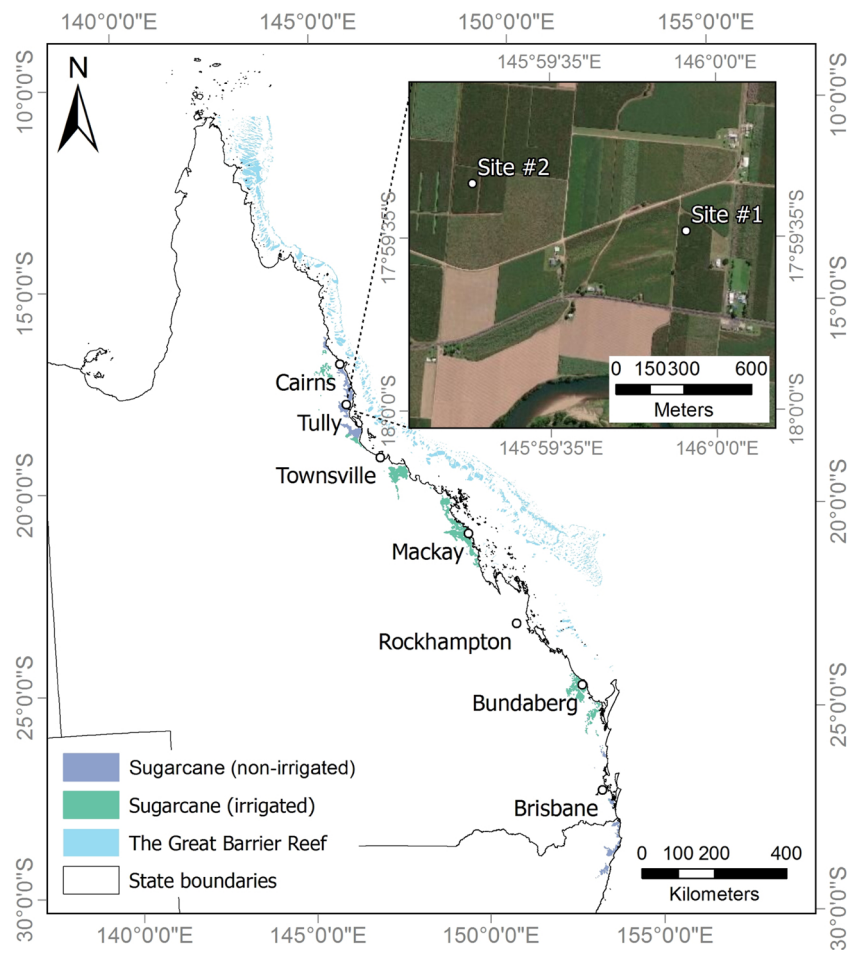


Fig. 1. Location of the study area in relation to sugarcane cultivation areas of Australia.

(i.e. one frame every two seconds). The RedEdge sensor also featured a downwelling light sensor and GPS module to allow image calibration to ground reflectance and georeferencing, respectively. In addition, a calibrated reflectance panel was imaged before and after each flight to assist with image calibration to ground reflectance. Utilizing a global shutter, the MicaSense RedEdge does not require a gimbal and, with the Hovermap, was fitted to the rear of the UAV with a simple anti-vibration mount (Fig. 4).

Each flight was planned using Global Mapper software (Global Mapper, 2019) and performed using Autopilot software (Hangar, 2019). To maximize point cloud density and canopy penetration, flight lines were positioned at 15 m intervals, while flight altitude for all Surveys in this study was set to 30 m above ground level (AGL). Further details of the UAV system and flight planning were provided in Sofonia et al. (2019b). Given that the study sites were part of an operational plantation, it was not practical to establish fixed ground control points (GCPs) over the duration of this study. Therefore, each scanning event was preceded by the placement of five AeroPoint (Propeller Aeropoints, 2019) GCPs with a <20 mm 3D resolution representatively distributed across the study area. The GCPs were later utilized to georeference multispectral imagery, and co-register LiDAR scans using SfM derived point clouds (Sofonia et al., 2019b).

2.4. UAV data processing

The methods for processing UAV-derived LiDAR point clouds and generating multispectral ground reflectance mosaics were described in Sofonia et al. (2019a) and Sofonia et al. (2019b). In addition, in this study, we used multispectral imagery to calculate 10 vegetation indices

described in Hunt et al. (2013) and Ballester et al. (2017) (Table 2), which were further evaluated in predicting sugarcane leaf N content and biomass. The majority of these vegetation indices have been previously used to derive leaf N content or biomass in cotton, maize, wheat, rice and sugarcane (Ballester et al., 2017; Hunt et al., 2013; Zheng et al., 2018a; Rahman and Robson, 2016; Basso et al., 2016). Vegetation indices (as opposed to reflectance bands) were also utilized in this study to minimize bidirectional reflectance distribution function (BRDF) effects (Huete et al., 1992) due to different UAV and illumination geometries of the six Surveys. The pixels representing ground were masked from multispectral imagery to utilize only areas covered by sugarcane for further analysis using mean thresholding of NDVI (Van der Walt et al., 2014).

Similarly, LiDAR scans, after pre-processing steps described in Sofonia et al. (2019a) and Sofonia et al. (2019b), were normalized with respect to the ground surface and used to extract 48 predictor variables within 2 m × 2 m biomass sampling plots (Fig. 2) in LasTools software (LAStools, 2015, Table 3), which previously confirmed to be useful in forest studies (Shendryk et al., 2016; Meng et al., 2018) and here were exclusively used for predicting sugarcane biomass.

Finally, we calculated predictor variables from multispectral imagery derived vegetation indices (Table 4). For this we extracted statistics for each of the leaf N and biomass sampling plots (Fig. 2). Thus, we generated 70 (i.e. seven statistical measures (Table 4) for 10 vegetation indices (Table 2) and 48 (Table 3) multispectral and LiDAR-derived predictors, respectively. There were no strong linear relationships between leaf N, biomass and predictor variables, hence we needed to use a multivariate method to generate reliable predictive models.

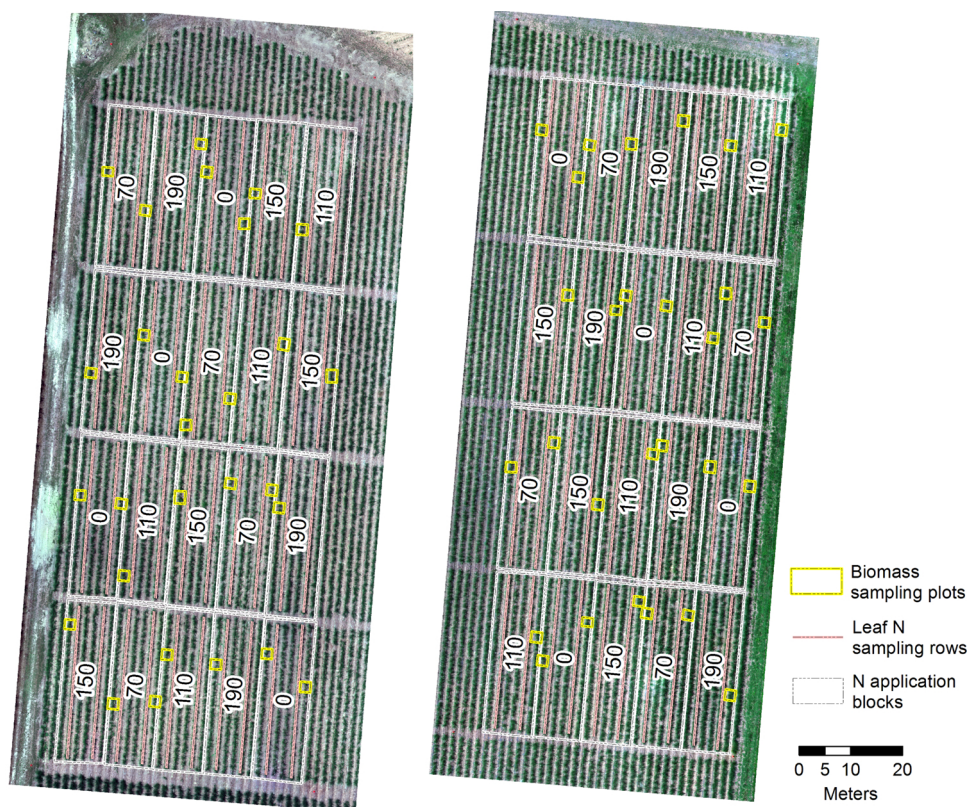


Fig. 2. The experimental design of a N trial in Site #1 (left) and Site #2 (right) with leaf N ($2\text{ m} \times 30\text{ m}$) and biomass ($2\text{ m} \times 2\text{ m}$) sampling plots highlighted in pink and yellow, respectively. (For interpretation of the references to color in this figure legend, the reader is referred to the web version of this article.)

Table 1
Survey dates and field samples collected.

Event	Survey date	Survey interval (days)	Days after harvest (DAH)	Leaf N sampled	Biomass sampled	Phenological phase
Survey #1	8/11/2017	–	58	No	No	Early growth
Survey #2	20/12/2017	42	100	Yes	No	Early growth
Survey #3	31/01/2018	42	142	Yes	No	Maturation
Survey #4	15/03/2018	43	185	Yes	No	Maturation
Survey #5	26/04/2018	42	227	Yes	No	Maturation
Survey #6	6/06/2018	41	268	No	Yes	Flowering

Note: Survey #1 was performed right after sugarcane fertilization and at the outset of the early growth phase, while Survey #3 was performed at the transition of early growth and maturation phenological phases.



Fig. 3. Examples of biomass sampling in 56 randomly distributed $2\text{ m} \times 2\text{ m}$ blocks across rows 1 and 6 (Fig. 2) showing (left) weighing of wet stems and (center) leaves and (right) disposal of sampled biomass.

2.5. Dimension reduction

The final data set for the total biomass dependent variable contained $n = 56$ observations and $p = 118$ predictors in total (i.e. 70 multispectral predictors and 48 LiDAR predictors in each of six Surveys). Since $p \gg n$, this placed us in the setting of high-dimensional

regression, a setting in which the standard ordinary least squares (OLS) breaks down. Furthermore, since the sample size of $n = 56$ was relatively small, methods that required a training/test split for biomass prediction were avoided, as further reduction in sample size would affect the model's ability to fit the data well, and test error would be sensitive to the initial choice for the split. Therefore, principal



Fig. 4. The DJI M600 Pro multirotor UAV equipped with Micasense RedEdge multispectral imaging sensor and Emesent Hovermap LiDAR sensor (left) on the ground and (right) shortly after takeoff.

Table 2

Vegetation indices calculated from various Micasense RedEdge reflectance band combinations.

Name	Equation
Normalized Difference Vegetation Index (NDVI)	$(NIR - R)/(NIR + R)$
Normalized Difference Red Edge Index (NDRE)	$(NIR - RE)/(NIR + RE)$
Green NDVI (GNDVI)	$(NIR - G)/(NIR + G)$
Enhanced Vegetation Index (EVI)	$2.5(NIR - R)/(NIR + 6R - 7.5B + 1)$
Modified Anthocyanin Content Index (MACI)	NIR/G
Optimized Soil Adjusted Vegetation Index (OSAVI)	$(1 + 0.16)(NIR - R)/(NIR + R + 0.16)$
Simplified Canopy Chlorophyll Content Index (SCCCI)	$NDRE/NDVI$
Transformed Chlorophyll Absorption and Reflectance Index (TCARI)	$3[RE - R - 0.2(RE/G)(RE/R)]/OSAVI$
Triangular Greenness Index (TGI)	$-0.5[(668 - 475)(R - G) - (668 - 560)(R - B)]$
Visible Atmospherically Resistant Index (VARI)	$(G^*R)/(G + R - B)$

R = red, G = green, B = blue, RE = red edge, NIR = near infrared.

Table 3

Predictor variables extracted from normalized (i.e. with respect to ground surface) LiDAR-derived point clouds.

Feature	Explanation
max	Maximum height
avg	Average height
qav	Average square height
std	Standard deviation of height
ske	Height skewness
kur	Height kurtosis
p05 to p95	5th to 95th height percentiles (increments of 5 percentiles)
b05 to b95	5th to 95th bincentiles ^a (increments of 5 bincentiles)
d00 ^b	The number of points between 0 (i.e. ground) and 0.01 m divided by the total number of points
d01 ^b	The number of points between 0.01 and 0.5 m divided by the total number of points
d02 ^b	The number of points between 0.5 and 1 m divided by the total number of points
d03 ^b	The number of points between 1 and 10 m divided by the total number of points

^a Fraction of points between ground and the height percentile.

^b Threshold values for d00, d01, d02 and d03 were defined to represent penetration of laser pulses at different height levels of sugarcane.

components analysis (PCA) was used to reduce the dimension of the data set down to a few predictors for each of the multispectral and LiDAR data sets respectively. The use of PCA, in turn, also allowed us to reduce multicollinearity (i.e. predictors that are correlated with other predictors) between predictor variables. Rather than selecting a subset of predictors, PCA constructs a set of linear combinations of all the predictors (i.e. principal components). The weights in each linear combination are chosen such that the principal component has largest possible variance and is orthogonal to all previous principal

Table 4

Predictor variables extracted from multispectral imagery derived vegetation indices.

Statistics	Explanation
max	Maximum value of all pixels within each plot
min	Minimum value of all pixels within each plot
avg	Average value of all pixels within each plot
std	Standard deviation of all pixels within each plot
p25	25th percentile of all pixels within each plot
p50	50th percentile of all pixels within each plot
p75	75th percentile of all pixels within each plot

Note: Sampling plots of leaf N and biomass are shown in Fig. 2.

components. By retaining only the first few principal components as predictors, the dimension of the data was greatly reduced while still capturing most of the variation it contained.

Since evaluating the fusion of multispectral and LiDAR predictors required estimating a model containing multispectral data only, one containing LiDAR only, and one containing both; PCA was undertaken on the multispectral and LiDAR data separately. For each data set, observations were grouped across time, resulting in 336 observations for each of 70 multispectral predictors, and 336 observations for 48 LiDAR predictors. To choose the number of components based only on the predictors and not the dependent variable, however many components explained 90% of the variance in the predictors were retained (Jolliffe, 2002, section 6.1.1). This corresponded to four and three principal components in the multispectral and LiDAR data sets, respectively. The same principal components model estimated here was also used for leaf N prediction, which will be discussed further in Section 2.7.

Given that the model was selected without reference to how well it

fitted the dependent variable, there was no capacity to choose a model which overfitted the noise. Therefore, our models are considered to be conservative, potentially underfitting the data and resulting in less predictive power. We were also able to get a sense of those predictor variables that contributed most to the results by examining which variables were weighted most heavily in forming the principal components; i.e. factor loadings (Jolliffe, 2002, chapter 7). The five most heavily weighted variables in the first principal component for the multispectral data were, in order, GNDVI (avg, p50, p25), NDVI (avg), and GNDVI (p75); with the second component being mainly composed of EVI (avg, p50, p75, p25) and SAVI (avg). For the LiDAR data, the first component was mainly composed of b55, avg, b60, p60, b50; and the second of kur, d00, p10, p15, std (Table 3).

2.6. Biomass prediction

The total of $n = 56$ observations of at-harvest biomass were used as a dependent variable. The prediction of this variable was based on four principal components from the multispectral data and three principal components from the LiDAR data in each of six Surveys (Table 1), yielding a total of 42 predictors (i.e. seven principal components at six time steps). Incorporating the entire time series for each principal component in the prediction of biomass was feasible through a finite distributed lag model. However, there would be three issues with such a model: (1) operationalizing the model for a prediction would require collecting six measurements at different times; (2) the number of samples and number of predictors would be close to each other, leading to statistical inefficiency; and (3) the model would only have capacity to give predictions close to the harvest date once all management decisions have already been made. Instead, our objective was to predict the at-harvest biomass independently in each of the six Surveys. For this a set of five different linear regression models in each of the six Surveys was estimated. Models 1 and 2 served as the benchmark, containing only NDVI (avg and max, respectively). Although NDVI usually saturates when vegetation coverage becomes dense, its use remains widespread in precision agriculture and is attractive because of the ease with which it is calculated (Gago et al., 2015). Models 3 and 4 used only the multispectral or LiDAR principal components, respectively. Model 5 was the multispectral/LiDAR fusion. In addition, each model was re-estimated including a term for the N application rate to determine whether the additional knowledge of the N fertilizer application rate improves predictive power. Model performance was evaluated using the adjusted coefficient of determination \bar{R}^2 . Ideally, estimates of out-of-sample R^2 would have been calculated through cross-validation, however this was limited due to the relatively small sample size employed in this study. Instead, \bar{R}^2 over R^2 was utilized given the number of predictors in each model ranged from two (intercept + NDVI) to eight (fusion model).

In this study, total, leaf and stem biomass as well as number of stems were measured independently. While total biomass was the most expedient quantity to measure in the field, it was also confirmed to be a good proxy for both stem and leaf biomass, as well as number of stems with $R^2 \geq 0.78$ (see Fig. 5). Therefore, our models were built to predict

total biomass only, as similar performance for both leaf and stem biomass was expected.

2.7. Leaf nitrogen prediction

In the assessment of leaf N content (%) as a dependent variable $n = 160$ observations were utilized (i.e. 40 observations in four time periods (i.e. Surveys #2–5)). As LiDAR derived information was not expected to be informative of leaf N content, we did not investigate LiDAR predictors and investigated only multispectral imagery derived vegetation indices of the leaves sampled in each Survey. While the set of 70 predictor variables constructed from the multispectral imagery derived vegetation indices were identical to those constructed for biomass prediction, the sampling plots used to generate predictor variables were different (Fig. 2). Since in each Survey there were 70 predictors for 40 observations of the dependent variable, a dimension reduction using PCA was also performed.

For each observation in the leaf N data set, the set of 70 predictors was projected through the principal components model estimated previously for multispectral predictors in biomass prediction. This resulted in the conversion of the 70 predictors into four principal components for each observation. Furthermore, the observations of the dependent variable were observed at multiple time periods, and as such, the data was grouped and estimated in a single model using the entire data set (unlike for biomass prediction). Fig. 6 displays the distributions of leaf N measured in each Survey and each fertilizer application rate. This shows that leaf N had a time trend which also needed to be considered.

Next, a linear regression was utilized in which leaf N content was regressed against each of the four contemporaneous principal components and a quadratic time trend. As for biomass, this model was benchmarked against models that used average and maximum NDVI respectively, and a model using the N application rate.

3. Results

3.1. Biomass prediction

3.1.1. Performance over time

For all models, \bar{R}^2 showed low goodness-of-fit at the beginning of the study (Survey #1), which increased in Surveys #2 and #3 (Fig. 7), then declined over time. All models performed comparably in Survey #1, corresponding to soon after the previous season's harvest date when vegetation was low.

Fig. 8 displays multispectral and LiDAR observations taken by the UAV during each Survey. Note that early in the season, blocks with different N application rates were relatively easy to differentiate, with blocks in which no fertilizer was applied clearly standing out. Individual rows of sugarcane were also clearly demarcated, however, the crop became more uniform in terms of measured reflectances and vegetation cover later in the season.

3.1.2. Multispectral vs LiDAR

Overall, sensor data from the multispectral, LiDAR, and the fusion of

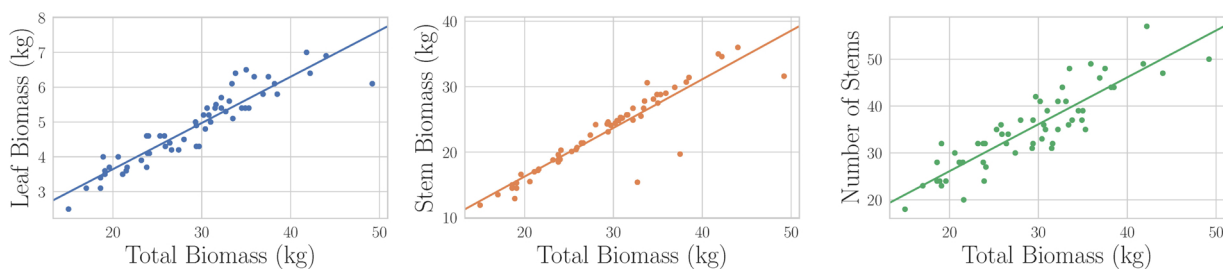


Fig. 5. Results of regression analysis between the total biomass against leaf biomass (left, $R^2 = 0.86$), stem biomass (center, $R^2 = 0.84$), and the number of stems (right, $R^2 = 0.78$) measured in 56, 2 m × 2 m plots.

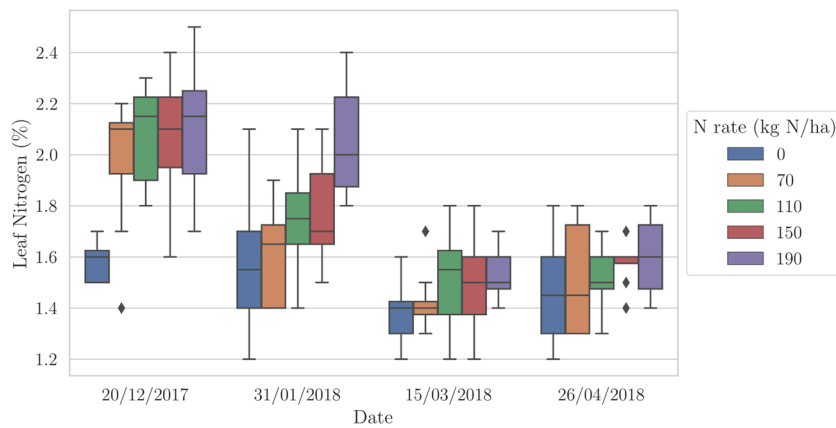


Fig. 6. Leaf N content (%) over time by fertilizer application rate as measured in 40 sampling plots at four time periods (i.e. Surveys #2–5).

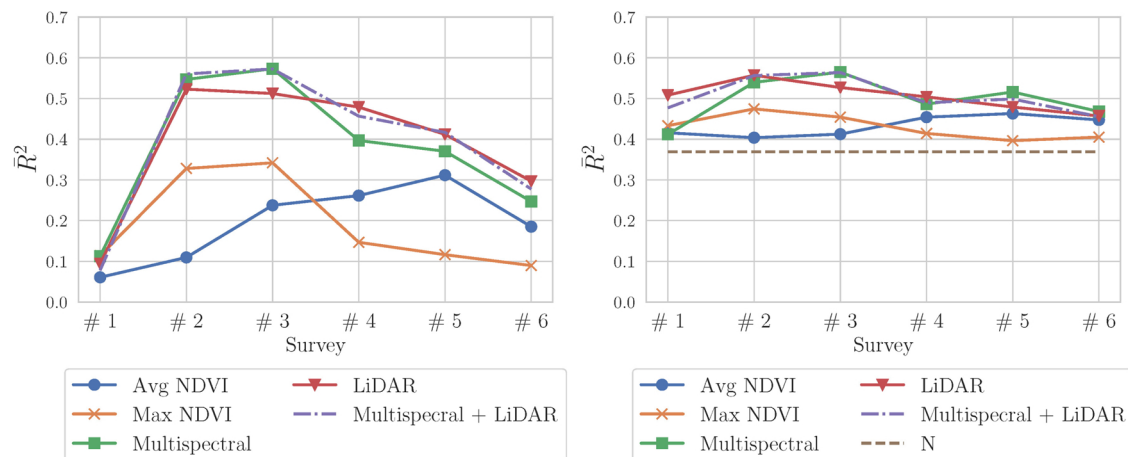


Fig. 7. \bar{R}^2 for each model in each Survey for biomass prediction. Left image corresponds to models without the N fertilization rate predictor, models on the right use that predictor.

both all performed comparably, with minor differences at different times in the growing season. Differences between a single sensor and the fusion of sensors can be tested statistically with an F -test, since each single sensor model was nested in the fusion model.³ However, a direct significance test for multispectral over LiDAR was not possible as the models were not nested within another.

In Surveys #2 and #3, the multispectral-only model performed slightly better than the LiDAR-only model, with an \bar{R}^2 approximately 0.06 higher in Survey #3. The fusion model did not perform statistically better than the multispectral-only model ($p = 0.22$ and $p = 0.41$ respectively for Survey #2 and #3). However, the fusion model performed statistically better than the LiDAR-only model at the 10% and 5% significance levels respectively ($p = 0.09$ and $p = 0.03$).

When predictive performance showed a decline closer to the harvest date, LiDAR models appeared to decline less quickly than multispectral models. During Surveys #4, #5, and #6, the fusion model did not perform significantly better than LiDAR-only ($p = 0.76$, 0.36 , and 0.63 , respectively). However, the fusion model outperformed the multispectral-only model at the 10% significance level in Surveys #4 and #5 ($p = 0.05$ and 0.08 , respectively).

³ A linear model with multispectral predictors only is nested in a linear model with both multispectral and LiDAR predictors, because the multispectral-only model can be retrieved by setting coefficients on the LiDAR predictors to zero. An F -test for significance of the fusion model over multispectral-only tests the hypothesis that all LiDAR coefficients are equal to zero.

3.1.3. Fertilization rate

The right hand side of Fig. 7 is analogous to the left hand side but where each model includes the additional predictor of the N fertilizer application rate. It also includes a model containing the N application rate only, without any sensor observations. Note that $\bar{R}^2 = 0.37$ for this model did not vary with time, since neither did the initial N application rate.

Once again, the models performed best in Surveys #2 and #3. However, the \bar{R}^2 values for the multispectral and fusion models did not change significantly in those time periods compared to these models without the additional predictor ($p = 0.91$ and 0.84 for multispectral and fusion respectively in Survey #3). In these Surveys, the sensors appeared to be able to account for variability due to fertilization differences without that predictor being included in the model. While predictions in Surveys #2 and #3 were unaffected by inclusion of a N rate predictor, the remaining Surveys were affected substantially. With this inclusion, predictive accuracy became more stable over time.

3.1.4. Benchmarks

The NDVI benchmarks performed worse than any sensor based model except in Survey #1, where they performed comparably. When equipped with the N rate, NDVI was still unable to outperform the principal components models in Surveys #2 and #3. Not only did the benchmarks perform worse than other sensor based models, but they performed worse than the model containing the N application rate only (Fig. 7); a model whose predictor is time invariant and does not require a UAV mission to collect. While NDVI is typically a strong predictor of

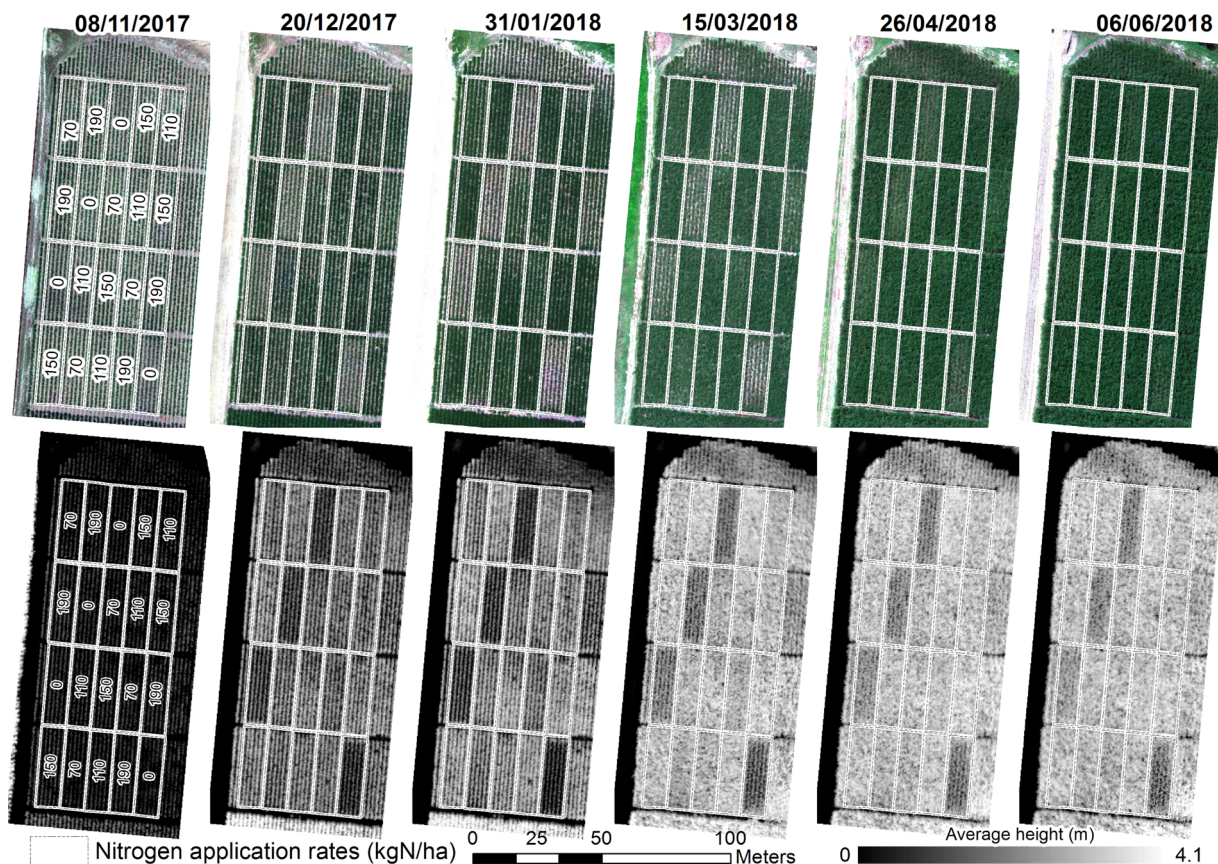


Fig. 8. Temporal variations of a *N* trial (Site #1) in terms of RGB imagery derived from RedEdge multispectral imagery (top) and average LiDAR-derived height (bottom).

vegetation biomass in remote sensing applications, and is in fact weighted heavily in the first principal component of our models, in this setting NDVI alone appeared to be a particularly poor predictor and must be augmented with additional predictors in order to achieve non-trivial predictive power.

3.2. Leaf nitrogen prediction

These results were somewhat analogous to the biomass estimation problem. The NDVI benchmarks (avg and max) performed similarly with $\bar{R}^2 \approx 0.39$ (Table 5). The model based on principal components of the multispectral imagery derived vegetation indices performed significantly better, with $\bar{R}^2 = 0.57$. A model containing the *N* rate as a predictor and no sensor predictors outperformed the benchmark with $\bar{R}^2 = 0.5$. The principal components model performed better by 0.07 with \bar{R}^2 . Inclusion of the *N* predictor in the principal components model did improve predictive power statistically ($p = 0.02$), but only increased \bar{R}^2 by 0.02.

Fig. 9 compares the observed and predicted values for leaf *N* content. Note that for low levels of measured leaf *N* content, the model tends to over-predict; whereas for high levels it tends to under-predict. This suggests that there are non-linearities present in the data and so fitting non-linear models (such as machine learning models) could improve predictive accuracy. Moreover, the observed leaf *N* content was rounded to the closest tenth decimal place, which limited the predictive capability of our model.

3.3. Comparison with independent estimates

The predictions from the best performing biomass prediction model (i.e. the multispectral predictors only model in the Survey #3 period)

Table 5

Regression output for prediction of leaf *N* content. Four models were estimated with the following predictors: (1) *N* fertilizer application rate, (2) average NDVI, (3) maximum NDVI, (4) four multispectral principal components. Each model included an intercept and a quadratic time trend.

Predictor	Model coefficients			
	(1)	(2)	(3)	(4)
<i>N</i> rate	0.0016***			
Avg NDVI		0.3298		
Max NDVI			0.7293	
PC1				0.0158**
PC2				-0.0372***
PC3				0.0422***
PC4				-0.0511***
Constant	1.4579***	1.3553***	0.9430	1.7774***
<i>t</i>	-0.0043**	-0.0044**	-0.0041*	-0.0043**
<i>t</i> ² ($\times 10^{-5}$)	3.887***	4.0***	3.872***	2.169***
Observations	160	160	160	160
<i>R</i> ²	0.513	0.397	0.400	0.586
\bar{R}^2	0.504	0.385	0.388	0.570

Note:

* $p < 0.1$.

** $p < 0.05$.

*** $p < 0.01$.

were further compared to the independent estimates produced by Sugar Research Australia (Section 2.1). First, the total biomass vs stem biomass relationship previously explored in Fig. 5 was compared. SRA estimated total biomass and stem biomass densities for each experimental block in tonnes per hectare; whereas our measurements were in

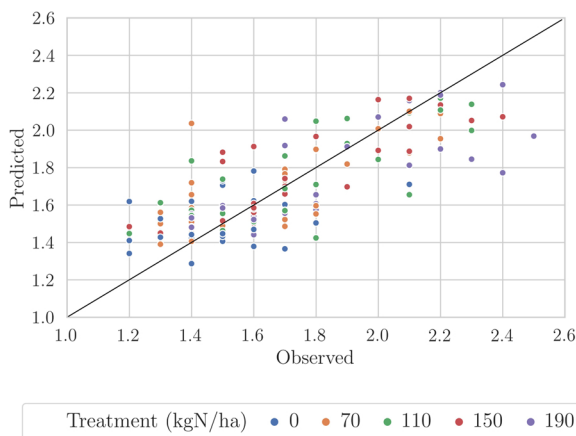


Fig. 9. Observed vs predicted leaf N content (%) derived using multispectral imagery principal components ($R^2 = 0.57$).

kilograms per $2\text{ m} \times 2\text{ m}$ plot. To put these on a comparable scale, each of our total and stem biomass measurements was transformed to be in t/ha by multiplying it by 2.5. Fig. 10 showed that both our and SRA's measures of total and stem biomass gave an almost identical linear relationship. Previously, in Fig. 5, it was found that the linear relationship had R^2 of 0.84. However, that plot contained three clear outliers, upon removal of which, the relationship became very strong, with $R^2 = 0.99$, which is approximately equal to the relationship found from SRA's data.

Next, the predictions of total biomass generated by our model were compared to SRA's estimates. Estimates for total biomass at the N application block level were constructed by predicting biomass in each $2\text{ m} \times 2\text{ m}$ plot in the paddock, then summing over all transects contained in each block. SRA estimated biomass density for each N trial block in t/ha. To convert our predictions in kilograms per block, where blocks were approximately $10\text{ m} \times 30\text{ m}$, to t/ha, our predictions were divided by 30. Fig. 10 illustrates the linear relationship between our model's predictions and SRA's estimates with an $R^2 = 0.65$. Notably, this line was not centered on the 45° line, as one would desire in order for these independent estimates to conform.

A key advantage of using UAV derived predictions as opposed to a currently adopted methodology for assessing N trials in sugarcane (Muchow et al., 1993) is that we can observe fine-scale ($2\text{ m} \times 2\text{ m}$) variations in crop biomass. Fig. 11 compares fine-scale predictions for the entire paddock to SRA's estimates, which are constant over each experimental block.

4. Discussion

Our results are of particular interest to nutrient-management programs aiming to deliver soil- and site-specific N fertilizer guidelines for sustainable sugarcane production, as both fine-scale biomass and leaf N content predictions are feasible when management interventions are still possible (i.e. as early as at 10 DAH). For example, split-application fertilization plans could be generated, where a base application of $2/3$ of the total N requirement is applied at the beginning of the growing season and topped up at around 100 or 142 DAH in under-performing or N deficient areas as identified by UAV-derived predictions. The adoption of a guided fertilization plan as opposed to a conventional practice of applying 100–160 kgN/ha (depending on soil organic carbon content) to sugarcane crops in the beginning of the growing season (Schroeder et al., 2010) may assist in better nutrient uptake by the crop, reducing environmental impact whilst preserving potential yield. However, there are practical limitations and additional costs associated with split N fertilizer application (Everingham et al., 2018). For example, the remainder of fertilizer would need to be applied closer to the onset of the wet season, thereby generating more environmental concerns in terms of the risk of N loss. It is also coupled with practical limitations as cane growers may not always be able to get machinery into the field due to the size of the crop at around 142 DAH.

Models for predicting leaf N content could be used to detect N deficient sugarcane and inform additional fertilization. The critical level of leaf N content was reported to be 1.9% and 1.8% during November to mid-January and mid-January to February in the Wet Tropics of Australia, respectively (Calcino et al., 2018). The field measured leaf N content (see Fig. 6) also suggested that in our study sugarcane blocks with 0 kgN/ha application rate were clearly N deficient at the time of Survey #2 (December), while blocks with 70 kgN/ha application rate became also N deficient by the time of Survey #3 (January) (see Fig. 6). However, leaf N content is sensitive to the environmental conditions experienced immediately prior to collecting the leaf sample (e.g. impact of pests, disease and moisture stress – either too wet or dry), which could have influenced the temporal changes more than age of the crop. To avoid subjectivity in generating fertilization guidelines based on either biomass or leaf N content predictions, optimum N requirements could be calculated using the method reported by Thorburn et al. (2017). Therefore, future studies should explore the potential of predicting optimum N requirements using UAV-derived data directly.

A relatively low performance of our models for biomass prediction ($\bar{R}^2 \leq 0.57$) could be explained by a small sample size of observations ($n = 56$) and large number of predictors ($p = 118$), which forced us to employ PCA, potentially underfitting the data and resulting in less

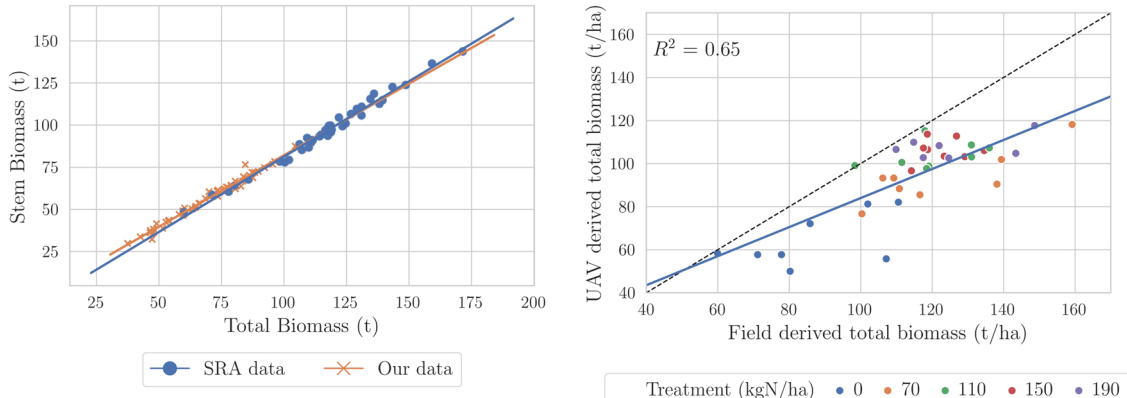


Fig. 10. Comparison of our biomass samples and total biomass predictions with those estimated by SRA. Total biomass vs stem biomass relationships for our field samples and SRA's estimates (left, $R^2 = 0.99$). Total biomass predicted by our UAV derived multispectral imagery model in Survey #3 vs SRA's estimate of total biomass in each experimental block (right, $R^2 = 0.65$).

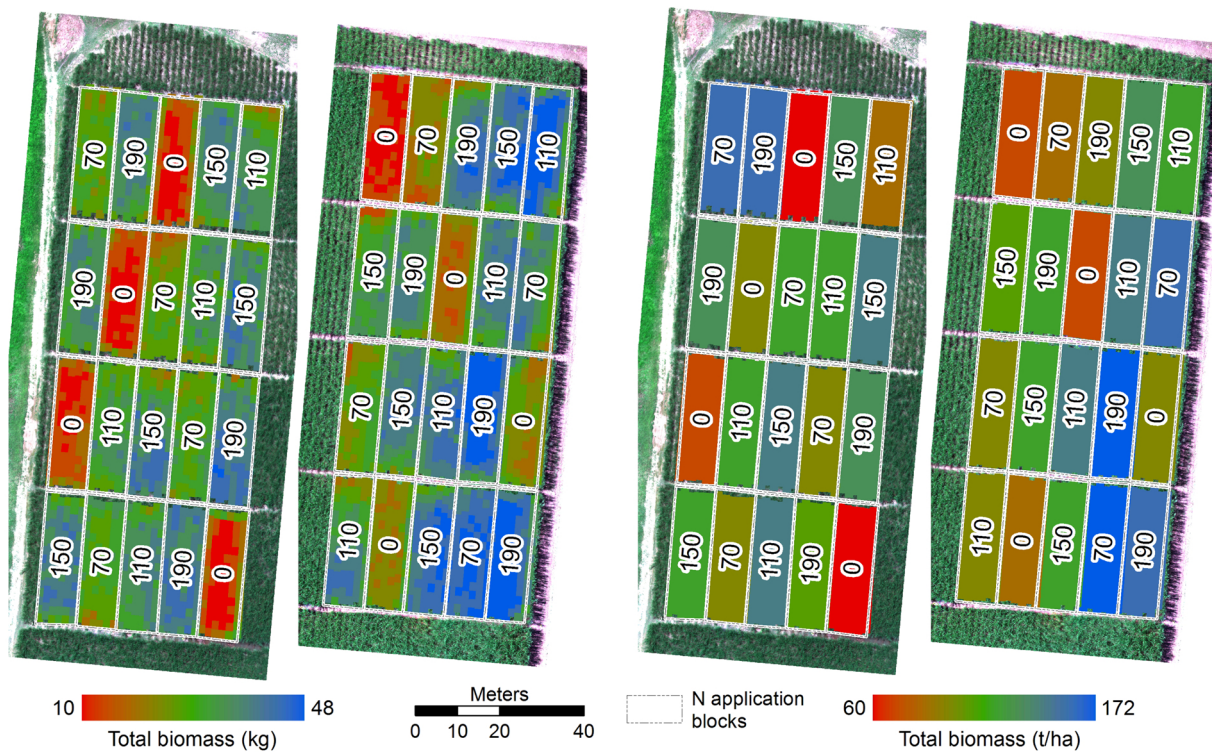


Fig. 11. Predicted total biomass in Sites #1 and #2 using multispectral imagery model at 142 DAH (i.e. Survey #3) in kg (left) and SRA's total biomass estimates in Sites #1 and #2 in t/ha (right).

predictive power. We also believe that the fine-scale approach in our study could also explain these results. To the best of our knowledge, the only two other studies (comparable to our work) that estimated sugarcane biomass using UAV-derived data were Sanches et al. (2018) and Sofonia et al. (2019b) achieving R^2 of 0.69 ($n = 45$) at 271 DAH and \bar{R}^2 of 0.71 ($n = 20$) at 268 DAH, respectively. However, the main difference is that both Sanches et al. (2018) and Sofonia et al. (2019b) related UAV-derived data to biomass measurements of relatively large field blocks of $10\text{ m} \times 12\text{ m}$ and $10\text{ m} \times 30\text{ m}$, respectively. These were much larger plot sizes compared to the ones measured in our study (i.e. $2\text{ m} \times 2\text{ m}$), thus were less susceptible to positioning errors associated with biomass measurements and UAV-derived predictors extraction.

In this study we found that predictive performance of sugarcane biomass peaked early in the season, at 100–142 (DAH), and declined closer to the harvest date, which was counter to some previous research. Sanches et al. (2018) showed that the best ($R^2 = 0.69$) predictive performance of at-harvest biomass using UAV-derived RGB imagery occurred near harvest (i.e. 271 DAH), and performance was lower ($R^2 = 0.63$) at 230 DAH. In contrast, in our study, worse predictive performance was observed closer to the harvest date ($\bar{R}^2 \approx 0.3$, Survey #6, 268 DAH) and better predictive performance at the transition of early growth and maturation phenological phases ($\bar{R}^2 = 0.55$, Survey #2, 100 DAH; $\bar{R}^2 = 0.57$, Survey #3, 142 DAH) when the highest growth rate occurred (Bull, 2000). Most likely this is because the difference in crop structure (i.e. height and density) and vegetation indices between N treatments disappear with the crop becoming older. While Sanches et al. (2018) did not assess the predictive power of their models prior to 230 DAH, similar to our results were reported by McCollam (2019) concluding that 100 days after fertilization is the most appropriate time for biomass prediction in sugarcane using UAV-derived NDVI (Pearson correlation (r) of 0.9). Given the reliability of early season (i.e. at 100–142 DAH) prediction of sugarcane biomass, they could be used to inform milling and harvest programs.

Our study also showed that the multispectral model performed slightly better ($\bar{R}^2 \leq 0.57$) than the LiDAR model ($\bar{R}^2 \leq 0.52$), with both

outperforming the NDVI benchmark ($R^2 \leq 0.34$) up to 142 DAH. However, the opposite was observed later in the season, with LiDAR performing better than multispectral, which could be partly explained by LiDAR's ability to penetrate dense canopy closer to the harvest date. Note in Fig. 8 that experimental blocks with low fertilizer application rates showed up clearly in both multispectral and LiDAR sensors. However, nearer to harvest the multispectral sensor had difficulty discriminating between application rates, while the LiDAR-derived average height image maintained these features. The fusion model did not perform statistically significantly better than the multispectral model at 100–142 DAH, nor better than LiDAR in subsequent periods. This is a contrasting result to other studies, where the fusion of LiDAR and hyperspectral information confirmed to improve predictions of biomass by R^2 of 0.05 (Wang et al., 2017; Luo et al., 2017). However, it is important to note that in Wang et al. (2017) ($n = 29$), unlike Luo et al. (2017) ($n = 33$), the accuracy assessment relied on in-sample unadjusted R^2 , producing R^2 of 0.83 and 0.88 when assessing LiDAR- and fusion-based (i.e. LiDAR in combination with hyperspectral imagery) models, respectively. By incorporating six additional predictors (i.e. hyperspectral imagery derived vegetation indices) in a LiDAR-based model, Wang et al. (2017) increased R^2 by 0.05. Similarly, in this study, the multispectral only model generated unadjusted R^2 of 0.6, while the fusion model resulted in R^2 of 0.63 in Survey #3 (DAH = 142), thus increasing R^2 by 0.03 for the additional three predictors (i.e. multispectral imagery derived principal components). This result is analogous to Wang et al. (2017). However, in-sample R^2 necessarily increases as one adds predictors to a model, so it is difficult to assess whether the increase in R^2 in Wang et al. (2017) was from adding informative predictors or if it was just an artefact of including more predictors in the model. In our study an F -test was performed to find that the increase in R^2 was statistically insignificant, while Wang et al. (2017) omitted such analysis, without concluding whether R^2 increase was statistically significant. Nevertheless, a relatively small sample size ($n = 56$) and positioning errors associated with biomass measurements and UAV-derived predictors extraction could partly explain low

performance of the fusion model in this study. Interestingly, our predictive models with N application rate as a predictor variable (see Fig. 7) did not improve biomass predictions at 100 and 142 DAH either, suggesting the ability of LiDAR and multispectral imagery to predict biomass in the absence of site-specific information.

Given similar performance of LiDAR and multispectral imagery in predicting sugarcane biomass at the fine scale and substantial price difference between those sensors, multispectral imagery could be considered as a preferred option for operationalization of biomass predictions. However, there are multiple advantages of a Hovermap LiDAR system that justify its use. Firstly, being a SLAM-based system, it does not require Global Navigation Satellite System (GNSS) and is therefore not subject to the same challenges as other LiDAR and multispectral systems that are dependent on satellite derived positional information (Whitehead and Hogenholtz, 2014). Secondly, the main metrics derived from LiDAR systems are height and density related and as such, their performance was not affected by, for example, canopy discoloration due to spraying or disease. Finally, LiDAR data can be collected irrespective of light conditions (during day or night) and usually post processed faster than photogrammetric data, which UAV-derived multispectral imagery relies on. Nevertheless, multispectral sensors could be effectively deployed at an altitude of up to 120 m (a common altitude limit for operating UAVs), thus allowing more efficient data collection over larger spatial scales. In contrast, a Hovermap LiDAR system is limited to a range of up to 100 m, with the point cloud accuracy being significantly affected at ranges of more than 50 m (Sofonia et al., 2019a).

Our models for predicting sugarcane biomass and leaf N content are rather site-specific and should be evaluated in other geographical areas and sugarcane varieties. Other environmental factors different than N treatments (e.g. weather conditions or the occurrence of pests or diseases) may also affect the LiDAR and multispectral derived measurements. Moreover, as the acquisition of UAV data is subject to weather conditions and usually limited to relatively small areas, it is important to investigate whether very-high resolution satellite imagery could be used to predict sugarcane biomass and leaf N content directly, or used as an intermediate to upscale UAV-derived predictions. Finally, collecting a larger sample of field-measured biomass ($n > 56$) over multiple time periods could potentially allow the use of more advanced predictive techniques (e.g. machine learning) to improve model performance. This would likely also require, however, the adoption of an automated biomass sampling procedure (Wendte et al., 2001) as opposed to the manual sampling used in this study. Unfortunately, there are no reliable biomass monitors available for sugarcane in the Wet Tropics of Australia.

The comparison of SRA-measured and our UAV-predicted biomass (see Fig. 10) revealed a strong bias. One explanation for this is that one of the methods contains a systematic bias and consistently under- or over-estimated total biomass. This is not surprising given the method for biomass measurements performed by SRA (Muchow et al., 1993) is basically an extrapolation of destructive sampling and weighting methods to the whole sugarcane block. Another explanation is that this bias was an artifact of the rescaling to put both measures in the same units. Mismeasurement of the transect or block areas will result in the slope of the line being not equal to 1, as will a sampling procedure that doesn't measure all biomass in a precise $2 \text{ m} \times 2 \text{ m}$ plot. Since sugarcane grows in rows, there are gaps between rows. In reality, these gaps may contain biomass growing out of neighboring rows. As we did not harvest this biomass, the area sampled may in fact be smaller than $2 \text{ m} \times 2 \text{ m}$. This would contribute to the bias between our estimates and those of SRA. Irrespective of which biomass estimate is more accurate in this comparison, the metric of interest to the cane growers is usually not biomass, but the quantity of commercial cane sugar (CCS) extracted (MSF Sugar, 2019). In this study we were unable to estimate CCS in $2 \text{ m} \times 2 \text{ m}$ plots used for biomass prediction. Therefore, future studies should focus on predicting CCS directly, as significant correlation

between CCS and biomass have been previously reported (Sandhu et al., 1997; Jackson et al., 1995).

5. Conclusions

This study demonstrated the potential of UAV LiDAR and multispectral imagery in predicting sugarcane biomass and leaf N content. Our model for predicting contemporaneous leaf N content (%) using multispectral imagery achieved an \bar{R}^2 of 0.57. We also found that performance of biomass predictions peaked early in the season, around 100–142 DAH, and declined closer to the harvest date with multispectral model performing slightly better ($\bar{R}^2 \leq 0.57$) than the LiDAR one ($\bar{R}^2 \leq 0.52$). However, the reverse was observed later in the season, with LiDAR performing slightly better than multispectral imagery. Interestingly, the fusion model did not perform significantly better than the multispectral imagery based model at 100–142 DAH, nor better than LiDAR in subsequent periods. Our models could be used to predict leaf N content and biomass in subsequent UAV surveys and thereby assist nutrient management programs in delivering N fertilizer guidelines for sustainable sugarcane production. Moreover, early season prediction of sugarcane biomass could be used to inform milling and harvest programs.

Authors' contribution

All authors contributed in a substantial way to the manuscript. Y.S. and J.S. conceived and proposed the experimental design and performed UAV surveys and field sampling. Y.S., J.S. and R.G. undertook the data analysis and wrote the original draft. Y.R. assisted with field sampling and data analysis. The materials and resources required were provided by P.T. and D.S., who also contributed to the review and editing of the paper and overall supervision of the project.

Conflict of interest

None declared.

Acknowledgements

This work was carried out within the “Great Barrier Reef” project of CSIRO Digiscape Future Science Platform. We would like to thank Dr. Scott Chapman from CSIRO for providing access to the multispectral imaging equipment as well as Dr. Stefan Hrabar and the rest of Emesent team for providing access to the Hovermap LiDAR sensor and support in conducting UAV surveys. The authors also thank Sugar Research Australia and the Department of Environment and Science for funding project #2015065 which established the experimental sites and the grower collaborator for providing site access.

Appendix A. Supplementary data

Supplementary data associated with this article can be found, in the online version, at <https://doi.org/10.1016/j.jag.2020.102177>.

References

- ABARES, 2018. Catchment Scale Land Use of Australia (December 2018). Retrieved from <https://data.gov.au/dataset/ds-dga-8d5d0a09-d100-407b-b326-6e775025feee/details>.
- Abdel-Rahman, E.M., Ahmed, F.B., Ismail, R., 2013. Random forest regression and spectral band selection for estimating sugarcane leaf nitrogen concentration using EO-1 Hyperion hyperspectral data. *Int. J. Rem. Sens.* 34 (2), 712–728.
- Adão, T., Hruška, J., Pádua, L., Bessa, J., Peres, E., Morais, R., Sousa, J., 2017. Hyperspectral imaging: a review on UAV-based sensors, data processing and applications for agriculture and forestry. *Rem. Sens.* 9 (11), 1110.
- Andrews, M., Raven, J., Lea, P., 2013. Do plants need nitrate? The mechanisms by which nitrogen form affects plants. *Ann. Appl. Biol.* 163 (2), 174–199.
- Bakker, H., 2012. Sugar Cane Cultivation and Management. Springer Science & Business

- Media.
- Ballester, C., Hornbuckle, J., Brinkhoff, J., Smith, J., Quayle, W., 2017. Assessment of in-season cotton nitrogen status and lint yield prediction from unmanned aerial system imagery. *Rem. Sens.* 9 (11), 1149.
- Basso, B., Fiorentino, C., Cammarano, D., Schulthess, U., 2016. Variable rate nitrogen fertilizer response in wheat using remote sensing. *Precis. Agric.* 17 (2), 168–182.
- Bendig, J., Bolten, A., Bennertz, S., Broscheit, J., Eichfuss, S., Bareth, G., 2014. Estimating biomass of barley using crop surface models (CSMs) derived from UAV-based RGB imaging. *Rem. Sens.* 6 (11), 10395–10412.
- Bendig, J., Yu, K., Aasen, H., Bolten, A., Bennertz, S., Broscheit, J., Gnyp, M.L., Bareth, G., 2015. Combining UAV-based plant height from crop surface models, visible, and near infrared vegetation indices for biomass monitoring in barley. *Int. J. Appl. Earth Observ. Geoinform.* 39, 79–87.
- Bocca, F.F., Rodrigues, L.H.A., Arraes, N.A.M., 2015. When do I want to know and why? Different demands on sugarcane yield predictions. *Agric. Syst.* 135, 48–56.
- Bull, T., 2000. The sugarcane plant. *Manual of Cane Growing.* pp. 71–83.
- Calcino, D., Schroeder, B., Panitz, J., Hurney, A., Skocaj, D., Wood, A., Salter, B., 2018. Australian Sugarcane Nutrition Manual. Retrieved from <https://sugarresearch.com.au/wp-content/uploads/2019/06/Australian-Sugarcane-Nutrition-Manual-June-2019.pdf>.
- Chingaryan, A., Sukkarieh, S., Whelan, B., 2018. Machine learning approaches for crop yield prediction and nitrogen status estimation in precision agriculture: a review. *Comput. Electron. Agric.* 151, 61–69.
- Christiansen, M., Laursen, M., Jørgensen, R., Skovsen, S., Gislum, R., 2017. Designing and testing a UAV mapping system for agricultural field surveying. *Sensors* 17 (12), 2703.
- De Souza, C.H.W., Lamparelli, R.A.C., Rocha, J.V., Magalhães, P.S.G., 2017. Height estimation of sugarcane using an unmanned aerial system (UAS) based on structure from motion (SfM) point clouds. *Int. J. Rem. Sens.* 38 (8–10), 2218–2230.
- Duan, T., Zheng, B., Guo, W., Ninomiya, S., Guo, Y., Chapman, S.C., 2017. Comparison of ground cover estimates from experiment plots in cotton, sorghum and sugarcane based on images and ortho-mosaics captured by UAV. *Funct. Plant Biol.* 44 (1), 169–183.
- Emesent, 2019. Retrieved from <https://emesent.io/>.
- Everingham, Y., Biggs, J., Schroeder, B., Skocaj, D., Thorburn, P., Sexton, J., 2018. How Much Will That Crop Need? Incorporating Climate Forecasting to Improve Nitrogen Management in the Wet Tropics. Sugar Research Australia Report.
- Everingham, Y., Inman-Bamber, N., Thorburn, P., McNeill, T., 2007. A Bayesian modeling approach for long lead sugarcane yield forecasts for the Australian sugar industry. *Austr. J. Agric. Res.* 58 (2), 87–94.
- FAO, 2019. Sugarcane Production in 2017, Crops/Regions/World list/Production Quantity (Pick Lists). UN Food and Agriculture Organization, Corporate Statistical Database (FAOSTAT). <http://www.fao.org/faostat/en/#data/QC>.
- Gago, J., Douthé, C., Coopman, R., Gallego, F., Ribas-Carbo, M., Flexas, J., Escalona, J., Medrano, H., 2015. UAVs challenge to assess water stress for sustainable agriculture. *Agric. Water Manag.* 153, 9–19.
- Global Mapper, 2019. Global Mapper – All-In-One GIS Software. Retrieved from <https://www.bluemarblegeo.com/products/global-mapper.php>.
- Hangar, 2019. Autopilot – Fly Like a Professional. Retrieved from <https://autoflight.hangar.com/autopilot>.
- Holman, F., Riche, A., Michalski, A., Castle, M., Wooster, M., Hawkesford, M., 2016. High throughput field phenotyping of wheat plant height and growth rate in field plot trials using UAV based remote sensing. *Rem. Sens.* 8 (12), 1031.
- Holzworth, D.P., Huth, N.I., deVoil, P.G., Zurcher, E.J., Herrmann, N.I., McLean, G., Chenu, K., van Oosterom, E.J., Snow, V., Murphy, C., et al., 2014. APSIM-evolution towards a new generation of agricultural systems simulation. *Environ. Model. Softw.* 62, 327–350.
- Huete, A., Hua, G., Qi, J., Chehbouni, A., Van Leeuwen, W., 1992. Normalization of multidirectional red and NIR reflectances with the SAVI. *Rem. Sens. Environ.* 41 (2–3), 143–154.
- Hunt Jr., E.R., Doraismamy, P.C., McMurtrey, J.E., Daughtry, C.S., Perry, E.M., Akhmedov, B., 2013. A visible band index for remote sensing leaf chlorophyll content at the canopy scale. *Int. J. Appl. Earth Observ. Geoinform.* 21, 103–112.
- Jackson, P., McRae, T., Hogarth, M., 1995. Selection of sugarcane families across variable environments. I. Sources of variation and an optimal selection index. *Field Crops Res.* 43 (2–3), 109–118.
- Jolliffe, I.T., 2002. Choosing a subset of principal components or variables. Principal Component Analysis. pp. 111–149.
- Jones, J.W., Antle, J.M., Basso, B., Boote, K.J., Conant, R.T., Foster, I., Godfray, H.C.J., Herrero, M., Howitt, R.E., Janssen, S., et al., 2017. Brief history of agricultural systems modeling. *Agric. Syst.* 155, 240–254.
- Keating, B.A., Thorburn, P.J., 2018. Modelling crops and cropping systems – evolving purpose, practice and prospects. *Eur. J. Agron.* 100, 163–176.
- Kefauver, S.C., Vicente, R., Vergara-Díaz, O., Fernandez-Gallego, J.A., Kerfal, S., Lopez, A., Melichar, J.Y., Serret Molins, M.D., Araus, J.L., 2017. Comparative UAV and field phenotyping to assess yield and nitrogen use efficiency in hybrid and conventional barley. *Front. Plant Sci.* 8, 1733.
- Kroes, J., Van Dam, J., Groenendijk, P., Hendriks, R., Jacobs, C., 2008. SWAP Version 3.2. Theory Description and User Manual. Technical Report Report1649, Alterra, Wageningen.
- LAStools, 2015. Retrieved from <https://rapidlasso.com/lastools/>.
- Leica Geosystems, 2019. Leica Viva GS16 – Self-Learning GNSS Smart Antenna. Retrieved from <https://leica-geosystems.com/products/gnss-systems/smart-antennas/leica-viva-gs16>.
- Luna, I., Lobo, A., 2016. Mapping crop planting quality in sugarcane from UAV imagery: a pilot study in Nicaragua. *Rem. Sens.* 8 (6), 500.
- Luo, S., Wang, C., Xi, X., Pan, F., Peng, D., Zou, J., Nie, S., Qin, H., 2017. Fusion of airborne LiDAR data and hyperspectral imagery for aboveground and belowground forest biomass estimation. *Ecol. Indic.* 73, 378–387.
- Maresma, Á., Ariza, M., Martínez, E., Lloveras, J., Martínez-Casasnovas, J., 2016. Analysis of vegetation indices to determine nitrogen application and yield prediction in maize (*Zea mays* L.) from a standard UAV service. *Rem. Sens.* 8 (12), 973.
- Matese, A., Toscano, P., Di Gennaro, S., Genesio, L., Vaccari, F., Primicerio, J., Belli, C., Zaldei, A., Bianconi, R., Gioli, B., 2015. Intercomparison of UAV, aircraft and satellite remote sensing platforms for precision viticulture. *Rem. Sens.* 7 (3), 2971–2990.
- McCollam, G., 2019. Correlating Nitrogen Application Rates in Sugarcane With Low-Cost Normalized Difference Vegetation Index (NDVI). Technical Report. Sustainable Agriculture Research & Education. Retrieved from <https://projects.sare.org/project-reports/fs14-282/>.
- Meng, R., Dennison, P.E., Zhao, F., Shendryk, I., Rickert, A., Hanavan, R.P., Cook, B.D., Serbin, S.P., 2018. Mapping canopy defoliation by herbivorous insects at the individual tree level using bi-temporal airborne imaging spectroscopy and LiDAR measurements. *Rem. Sens. Environ.* 215, 170–183.
- Micasense, 2019. Retrieved from <https://www.micasense.com/>.
- Miphokasap, P., Honda, K., Vaiphasa, C., Souris, M., Nagai, M., 2012. Estimating canopy nitrogen concentration in sugarcane using field imaging spectroscopy. *Rem. Sens.* 4 (6), 1651–1670.
- Miphokasap, P., Wannasiri, W., 2018. Estimations of nitrogen concentration in sugarcane using hyperspectral imagery. *Sustainability* 10 (4), 1266.
- Mitchell, A., Reghenzani, J., Furnas, M., De'ath, G., Brodie, J., Lewis, S., 2007. Nutrients and Suspended Sediments in the Tully River: Spatial and Temporal Trends. ACTFR Report, 6(06).
- Molijn, R.A., Iannini, L., Rocha, J.V., Hanssen, R.F., 2018. Ground reference data for sugarcane biomass estimation in São Paulo state, Brazil. *Sci. Data* 5, 180150.
- Morel, J., Todoroff, P., Bégué, A., Bury, A., Martiné, J.-F., Petit, M., 2014. Toward a satellite-based system of sugarcane yield estimation and forecasting in smallholder farming conditions: a case study on Réunion Island. *Rem. Sens.* 6 (7), 6620–6635.
- MS, Sugar, 2019. Cane Pricing Guide: For Growers Who Nominate MSF Marketing as Their Pool Manager. Retrieved from <https://www.msfsugar.com.au/wp-content/uploads/2016/08/MSF-Sugar-Cane-Pricing-Guide-2016.pdf>.
- Muchow, R., Robertson, M., Wood, A., 1996. Growth of sugarcane under high input conditions in tropical Australia. II. Sucrose accumulation and commercial yield. *Field Crops Res.* 48 (1), 27–36.
- Muchow, R., Wood, A., Spillman, M., Robertson, M., Thomas, M., 1993. Field techniques to quantify the yield-determining processes in sugarcane. 1. Methodology. In: Proceedings of the 15th Conference of the Australian Society of Sugar Cane Technologists. Australian Society of Sugar Cane Technologists.
- Mulla, D.J., 2013. Twenty five years of remote sensing in precision agriculture: key advances and remaining knowledge gaps. *Biosyst. Eng.* 114 (4), 358–371.
- Nex, F., Remondino, F., 2014. UAV for 3D mapping applications: a review. *Appl. Geomat.* 6 (1), 1–15.
- Promburom, P., Jintrawet, A., Ekasingh, M., 2001. Estimating sugarcane yields with O-Y Thai interface. *Proceedings International Society of Sugar Cane Technologists*, Vol. 24 81–86.
- Propeller Aeropoints, 2019. Retrieved from <https://www.propellernorthfro.com.au/>.
- Rahman, M.M., Robson, A.J., 2016. A novel approach for sugarcane yield prediction using landsat time series imagery: a case study on Bundaberg region. *Adv. Rem. Sens.* 5 (2).
- Reboldi, F., Atzberger, C., Savin, I., Rojas, O., 2013. Using low resolution satellite imagery for yield prediction and yield anomaly detection. *Rem. Sens.* 5 (4), 1704–1733.
- Romheld, V., 2012. Diagnosis of deficiency and toxicity of nutrients. Marschner's Mineral Nutrition of Higher Plants. Elsevier, pp. 299–312.
- Sanches, G.M., Duft, D.G., K“ollin, O.T., Luciano, A.C.d.S., De Castro, S.G.Q., Okuno, F.M., Franco, H.C.J., 2018. The potential for RGB images obtained using unmanned aerial vehicle to assess and predict yield in sugarcane fields. *Int. J. Rem. Sens.* 39 (15–16), 5402–5414.
- Sandhu, D., Saini, G., et al., 1997. Inter-relationships among cane yield and commercial cane sugar and their component traits in autumn plant crop of sugarcane. *Euphytica* 95 (1), 109–113.
- Schirrmann, M., Giebel, A., Gleiniger, F., Pflanz, M., Lentschke, J., Dammer, K.-H., 2016. Monitoring agronomic parameters of winter wheat crops with low-cost UAV imagery. *Rem. Sens.* 8 (9), 706.
- Schroeder, B., Hurney, A., Wood, A., Moody, P., Allsopp, P., 2010. Concepts and value of the nitrogen guidelines contained in the Australian sugar industry's 'six easy steps' nutrient management program. *Proceedings of the International Society of Sugar Cane Technologists*, Vol. 27.
- Shendryk, I., Broich, M., Tulbure, M.G., McGrath, A., Keith, D., Alexandrov, S.V., 2016. Mapping individual tree health using full-waveform airborne laser scans and imaging spectroscopy: a case study for a floodplain eucalypt forest. *Rem. Sens. Environ.* 187, 202–217.
- Sofonia, J., Phinn, S., Roelfsema, C., Kendoul, F., Rist, Y., 2019a. Modelling the effects of fundamental UAV flight parameters on LiDAR point clouds to facilitate objectives-based planning. *ISPRS J. Photogram.* *Rem. Sens.* 149, 105–118.
- Sofonia, J., Shendryk, Y., Phinn, S., Roelfsema, C., Kendoul, F., Skocaj, D., 2019b. Monitoring sugarcane growth response to varying nitrogen application rates: a comparison of UAV SLAM LiDAR and photogrammetry. *Int. J. Appl. Earth Observ. Geoinform.* 82, 101878.
- Som-ard, J., Hossain, M.D., Ninsawat, S., Veerachitt, V., 2018. Pre-harvest sugarcane yield estimation using UAV-based RGB images and ground observation. *Sugar Tech* 20 (6), 645–657.
- Thorburn, P., Biggs, J., Webster, A., Biggs, I., 2011. An improved way to determine nitrogen fertiliser requirements of sugarcane crops to meet global environmental challenges. *Plant Soil* 339 (1–2), 51–67.

- Thorburn, P., Biggs, J.S., Palmer, J., Meier, E.A., Verburg, K., Skocaj, D.M., 2017. Prioritizing crop management to increase nitrogen use efficiency in Australian sugarcane crops. *Front. Plant Sci.* 8, 1504.
- Van der Walt, S., Schröder, J.L., Nunez-Iglesias, J., Boulogne, F., Warner, J.D., Yager, N., Gouillart, E., Yu, T., 2014. Scikit-image: image processing in Python. *PeerJ* 2, e453.
- Velodyne, 2018. VLP-16 User Manual. Retrieved from <https://velodynelidar.com/downloads/>.
- Vigneau, N., Ecarnot, M., Rabatel, G., Roumet, P., 2011. Potential of field hyperspectral imaging as a non-destructive method to assess leaf nitrogen content in Wheat. *Field Crops Res.* 122 (1), 25–31.
- Wang, C., Nie, S., Xi, X., Luo, S., Sun, X., 2017. Estimating the biomass of maize with hyperspectral and LiDAR data. *Rem. Sens.* 9 (1), 11.
- Wendte, K.W., Skotnikov, A., Thomas, K.K., 2001. Sugar cane yield monitor. US Patent 6, 272,819.
- Whitehead, K., Hugenholtz, C.H., 2014. Remote sensing of the environment with small unmanned aircraft systems (UASs). Part 1. A review of progress and challenges. *J. Unmanned Vehicle Syst.* 2 (3), 69–85.
- Yu, B., 1998. Rainfall erosivity and its estimation for Australia's tropics. *Soil Res.* 36 (1), 143–166.
- Zhang, C., Kovacs, J.M., 2012. The application of small unmanned aerial systems for precision agriculture: a review. *Precis. Agric.* 13 (6), 693–712.
- Zheng, H., Cheng, T., Li, D., Yao, X., Tian, Y., Cao, W., Zhu, Y., 2018a. Combining unmanned aerial vehicle (UAV)-based multispectral imagery and ground-based hyperspectral data for plant nitrogen concentration estimation in rice. *Front. Plant Sci.* 9, 936.
- Zheng, H., Li, W., Jiang, J., Liu, Y., Cheng, T., Tian, Y., Zhu, Y., Cao, W., Zhang, Y., Yao, X., 2018b. A comparative assessment of different modeling algorithms for estimating leaf nitrogen content in winter wheat using multispectral images from an unmanned aerial vehicle. *Rem. Sens.* 10 (12), 2026.
- Zhou, X., Zheng, H., Xu, X., He, J., Ge, X., Yao, X., Cheng, T., Zhu, Y., Cao, W., Tian, Y., 2017. Predicting grain yield in rice using multi-temporal vegetation indices from UAV-based multispectral and digital imagery. *ISPRS J. Photogram. Rem. Sens.* 130, 246–255.